

## Estimation of direct-seeded guayule cover, crop coefficient, and yield using UAS-based multispectral and RGB data

Diaa Eldin M. Elshikha<sup>a,d,\*</sup>, Douglas J. Hunsaker<sup>b</sup>, Peter M. Waller<sup>a</sup>, Kelly R. Thorp<sup>b</sup>, David Dierig<sup>c</sup>, Guangyao Wang<sup>c</sup>, Von Mark V. Cruz<sup>c</sup>, Matthew E. Katterman<sup>a</sup>, Kevin F. Bronson<sup>b</sup>, Gerard W. Wall<sup>b</sup>, Alison L. Thompson<sup>b</sup>

<sup>a</sup> Biosystems Engineering Dept., The University of Arizona, Tucson, AZ 85721, United States

<sup>b</sup> USDA-ARS, Arid Land Agricultural Research Center, Maricopa, AZ 85138, United States

<sup>c</sup> Bridgestone Americas, Inc, 4140 West Harmon Rd, Eloy, AZ 85131, United States

<sup>d</sup> Agricultural Engineering Dept., Faculty of Agriculture, Mansoura University, Al Mansoura, Egypt

### ARTICLE INFO

Handling editor - Xiying Zhang

#### Keywords:

Crop coefficient  
Furrow  
Guayule  
Irrigation  
Resin  
Rubber  
Subsurface drip

### ABSTRACT

Guayule (*Parthenium argentatum*, A. Gray), a perennial desert shrub, produces high-quality natural rubber and is targeted as a domestic natural rubber source in the U.S. While commercialization efforts for guayule are on-going, crop management requires plant growth monitoring, irrigation requirement assessment, and final yield estimation. Such assistance for guayule management could be provided with remote sensing (RS) data. In this study, field and RS data, collected via drones, from a 2-year guayule irrigation experiment conducted at Maricopa, Arizona were evaluated. In-season field measurements included fractional canopy cover ( $f_c$ ), basal ( $K_{cb}$ ) and single ( $K_c$ ) crop coefficients, and final yields of dry biomass (DB), rubber (RY), and resin (ReY). The objectives of this paper were to compare vegetations indices from MS data (NDVI) and RGB data (triangular greenness index, TGI); and derive linear prediction models for estimating  $f_c$ ,  $K_{cb}$ ,  $K_c$ , and yield as functions of the MS and RGB indices. The NDVI and TGI showed similar seasonal trends and were correlated at a coefficient of determination ( $r^2$ ) of 0.52 and a root mean square error (RMSE) of 0.11. The prediction of measured  $f_c$  as a linear function of NDVI ( $r^2 = 0.90$ ) was better than by TGI ( $r^2 = 0.50$ ). In contrast to TGI, the measured  $f_c$  was highly correlated with estimated  $f_c$  based on RGB image evaluation ( $r^2 = 0.96$ ). Linear models of  $K_{cb}$  and  $K_c$ , developed over the two years of guayule growth, had similar  $r^2$  values vs NDVI ( $r^2 = 0.46$  and  $0.41$ , respectively) and vs TGI ( $r^2 = 0.48$  and  $0.40$ , respectively). Final DB, RY, and ReY were predicted by both NDVI ( $r^2 = 0.75$ ,  $0.53$ , and  $0.70$ , respectively) and TGI ( $r^2 = 0.72$ ,  $0.48$ , and  $0.65$ , respectively). The RS-based models enable estimation of irrigation requirements and yields in guayule production fields in the U.S.

### 1. Introduction

Guayule (*Parthenium argentatum*, A. Gray), a perennial shrub native to the desert of northcentral Mexico and southern Texas, produces high-quality natural rubber used in tire manufacturing, as well as natural resin for other industrial products (Rasutis et al., 2015). Commercialization efforts for guayule have been on-going in the US Southwest for many years (Ray et al., 2010). Acreages of traditional crops in the region, such as cotton and alfalfa, continue to decline (Lahmers and Eden, 2018), coinciding with on-going drought and associated water shortage concerns (Mpanga and Idowu, 2021). Guayule is seen as a suitable water-savings alternative crop due to its ability to withstand prolonged

periods without water application (Allen et al., 1987). Nevertheless, guayule production in the area remains limited. Unlike annual crops, guayule is grown for a two-year period before harvest, which can complicate crop management decisions. Thus, among the needs for increasing commercial guayule production is having adequate technologies that assist growers with crop and irrigation management. Today's growers are already using tools such as remote sensing and scientific irrigation scheduling for traditional crops. These applications should be provided for guayule crop management, as well.

During 2018–2020, a guayule experiment was conducted at Maricopa, Arizona to evaluate the growth and yield response to variable water application rates using subsurface drip (SDI) and furrow irrigation

\* Corresponding author at: Biosystems Engineering Dept., The University of Arizona, Tucson, AZ 85721, United States.

E-mail address: [diaaelshikha@arizona.edu](mailto:diaaelshikha@arizona.edu) (D.E.M. Elshikha).

for direct-seeded guayule (Elshikha et al., 2021). During the two years of continuous growth, guayule crop evapotranspiration ( $ET_c$ ) was calculated for two well-watered treatments with furrow and SDI using a soil water balance method. The  $ET_c$  data for the treatments were used to assess the single ( $K_c$ ), basal ( $K_{cb}$ ), and soil evaporation ( $K_e$ ) coefficients over the two-year study. In addition, time-based, growth stage curves of  $K_c$  and  $K_{cb}$  were developed for the spring-planted guayule, providing the first known guayule curves for applications using the FAO56 procedures (Allen et al., 1998). However, the limitations of these locally-derived crop coefficients and the related plant growth parameters (PGP), e.g., fractional canopy cover ( $f_c$ ) are that they may be relatively site and climate specific and, thus, not necessarily directly transferrable to other cropping areas and conditions. For example, guayule is known to have two distinctive planting seasons (fall and spring) in Arizona (Coffelt and Ray, 2010; Hunsaker and Elshikha, 2017). Because of different climatic conditions, time-based  $K_{cb}$  and  $K_c$  curves are likely to be different for spring and fall plantings, especially during guayule's first year of growth. In spring, plants are subjected to increasing climatic conditions (temperature and solar radiation), while in fall they experience declining climatic effects during winter months. Even when guayule is planted in the same season, initial growth and development could vary in time due to different seasonal climatic conditions.

Remote sensing (RS) of vegetation index (VI) offers a means to estimate  $f_c$  and crop coefficients without a reliance on time-driven curves (Hunsaker et al., 2005; Johnson and Trout, 2012). The foundational basis is that certain VIs, mathematical combinations of two or more spectral bands, are shown to be highly correlated to green vegetation and therefore correlate well to parameters such as  $f_c$  and  $K_{cb}$  (Pocas et al., 2020). Adapting the locally-derived guayule  $K_c$  and  $K_{cb}$  data from Elshikha et al. (2021) based on VI would be more practical for use with a different planting date, planting method, and climate. Remote sensing data can be collected via satellites, ground sensors, airplanes or drones carrying multispectral (MS) sensors and RGB (Red-Green-Blue) cameras. Certain RS VIs, in the form of normalized difference vegetation index (NDVI) and the soil adjusted vegetation index (SAVI), have been utilized to predict  $K_{cb}$  and improve  $ET_c$  estimation and irrigation planning (Bausch, Neale, 1989; Bausch, 1995; Jayanthi et al., 2001; Johnson et al., 2003; Neale et al., 2003; Hunsaker et al., 2005; Johnson and Trout, 2012). The studies also reported the capability of RS-based  $K_{cb}$  to account for the variation in plant growth caused by variable weather conditions and plant health (disease, weed and insect infestation). Some studies have indicated that MS VIs can be used to predict PGP, such as  $f_c$ , and forecast final biomass and yield (Vina et al., 2004; Mondal and Basu, 2009; Li et al., 2010; Coelho et al., 2018; Zhang et al., 2021; Ji et al., 2021). Although ground-based sensors are simple to operate, they cover only small areas of the field, and they are time-consuming and labor-intensive. On the other hand, satellite imagery provides large coverage area. However, if RS data is used for management decisions, high spatial and temporal resolution is often required, which may not be available through satellites. Aerial data through helicopters and airplanes are limited by the cost and unexpected changes in weather conditions.

Some of the MS-based platform limitations may be overcome through the use of unmanned aircraft systems (UAS), which have gained the interest of researchers and farmers due to their flexibility and high spatial resolution (Yan et al., 2019; Campos et al., 2019; Xu et al., 2020). UAS carrying multispectral and RGB (red, green, blue) cameras have been indicated to be appropriate for crop growth and yield monitoring (Lu, 2005; Torres-Sanchez et al., 2014; Huang et al., 2016; Kanning et al., 2018; Li et al., 2018a; Hlatshwayo et al., 2019; Yang et al., 2020; Zhang et al., 2021). Many studies have shown that RGB images can result in accurate estimation of  $f_c$  for a wide range of vegetation coverage and using various image resolutions (Chen et al., 2016; Duan et al., 2017; Li et al., 2018b; Yan et al., 2019; Jiang et al., 2020). Studies by Hunt Jr. et al. (2005, 2011, 2013) have indicated that the triangular green index (TGI), an RGB index, is well-correlated with plant

chlorophyll content and biomass. As a low-cost alternative to MS data, RGB images have been utilized to predict multispectral indices such as NDVI (Costa et al., 2020). However, the vast majority of prediction equations available for PGP (e.g.,  $f_c$ , and biomass) are based on MS VI indices (such as NDVI). Therefore, MS-based PGP-VI relations are already available for many crops, whereas RGB-based VI relations are less developed.

Another RS application that could potentially assist guayule growers with decision-making is prediction of final yields using MS and/or RGB data. Such information could help growers plan post-harvest logistical operations (e.g., scheduling transportation and storage facilities). Currently, estimation of guayule dry biomass (DB), rubber yield (RY), and resin yield (ReY) can be made prior to final harvest by collecting whole plant samples that are then dried, ground, and analyzed for the secondary rubber and resin products (Cornish et al., 2013). Some empirical relations have been developed to non-destructively estimate guayule yields based on plant volume measurements (Downes and Tonnet, 1985). In either case, these methods are more cumbersome, time consuming, and costly compared to using predictions based on inexpensive drone data acquisitions. The MS (NDVI) and RGB (TGI) indices have been used to estimate biomass and final yields for other crops (Hunt Jr. et al., 2005; Zhao et al., 2007; Brandao et al., 2015; Ji et al., 2021) but not for guayule.

As indicated, no RS methods have yet been adapted for irrigation and crop management of guayule. Therefore, a primary goal of this study is to provide an initial indication of NDVI and TGI applications in guayule. The specific objectives of this study are to (1) compare MS (NDVI) and RGB (TGI) trends and relationships in guayule; (2) develop VI-based and RGB image-based estimates of  $f_c$ ; (3) derive  $K_{cb}$  and  $K_c$  as functions of NDVI and TGI; and (4) develop guayule DB, RY, and ReY estimation equations for NDVI and TGI.

## 2. Materials and methods

### 2.1. Irrigation experiment

An irrigation experiment was conducted to study the effects of irrigation rate and method (subsurface drip [SDI] and furrow [F]) on the growth and yield of direct-seeded guayule (Elshikha et al., 2021). The guayule crop was grown for  $\approx$ two years until harvested. It was planted in late-Apr. 2018 at two-field sites in Arizona: one site was a 1.0-ha field at The University of Arizona, Maricopa Agricultural Center in Maricopa, Arizona (32.67 °N lat; 111.63 °W long; 482 m a.s.l.) and the other site was in Eloy, Arizona. Because RS data collection was very limited at the Eloy site, that field experiment is not included in this paper. The Maricopa field consisted of 18, 75-m long plots that were 6.1-m wide (six rows). Irrigation treatments, irrigation scheduling, and field data collection are described in Elshikha et al. (2021). Briefly, the guayule experiment included five treatments of irrigation amount (50–150% of estimated  $ET_c$ , denoted as D50-D150) using SDI and one treatment with 100% of  $ET_c$  using furrow irrigation (denoted as F100). The experimental design was a randomized complete block in three blocks. Actual  $ET_c$  was measured for the D100 and F100 treatments using periodic measurements of soil water content via neutron moisture meter and measured irrigation and precipitation amounts. The daily soil water balance methodologies used to derive  $K_c$ ,  $K_{cb}$ , and  $K_e$  based on the  $ET_c$  measurements were also described by Elshikha et al. (2021). The guayule was harvested in March 2020 after  $\approx$  23 months of growth. Experimental measurements of guayule cover and yields are described in Section 2c below.

## 2.2. Remote sensing platforms and vegetations indices

Remote sensing data were collected during the 2018–2020 irrigation experiment at Maricopa using two RS platforms. The first platform was a drone (Phantom 4 Pro V2.0,<sup>1</sup> Da-Jiang Innovations [DJI], Nanshan District, China), which collected RGB images at 30–60 m above ground level. The drone was equipped with a 25-mm, 20-megapixel CMOS detector with a mechanical shutter. The images (R, G and B values) were used to calculate TGI by Pix4D 2019 (a photogrammetry software technology, Prilly, Switzerland), which is based on Hunt Jr. et al. (2011) as follows:

$$TGI = -0.5 \times [(668-475) (R - G) - (668-560) (R - B)] \quad (1)$$

where blue (B), green (G), and red (R) are the waveband reflectance values for the respective bands. The 668, 475 and 560 are centers of the wavebands for the R, G and B bands, respectively. RGB images were used to estimate  $f_c$  in each treatment plot using the following steps: 1) conversion of RGB image data to hue, saturation, and intensity (HSI) color space (Thorp and Dierig, 2011); 2) classification of the hue channel into plant and soil classes via an expectation maximization classification algorithm in OpenCV; and 3) dividing the number of pixels classified as plant by the total number of pixels in each plot.

The second platform was a drone (Inspire 2, DJI, Nanshan District, China) carrying a multispectral MicaSense sensor: a RedEdge sensor which had five bands (Blue [475 nm], Green [560 nm], Red [668 nm], Red Edge [717 nm], Near Infrared [nir, 842 nm]), which was replaced with a newer MicaSense Altum sensor with the same five bands and a thermal infrared (LWIR) band (8000–14000 nm). Crop canopy reflectance data were used to compute the commonly-used NDVI (Tucker, 1979), which was developed to maximize sensitivity to the vegetation characteristics while minimizing soil background reflectance and atmospheric effects. The NDVI was computed by Eq. (2), utilizing the information in the red (668 nm center, 16 nm bandwidth) and nir (842 nm center, 57 nm bandwidth).

$$NDVI = (\rho_{nir} - \rho_{red}) / (\rho_{nir} + \rho_{red}) \quad (2)$$

where  $\rho_{nir}$  and  $\rho_{red}$  are spectral reflectance in the nir and red regions of the electromagnetic spectrum, respectively.

The RS data collection for both platforms was begun in late Jun. 2018 and continued through early Mar. 2020 (just prior to harvest). Acquisition intervals for the two platforms varied from  $\approx$ weekly to tri-weekly, where the longer intervals occurred during late fall through late winter 2018–2019, when guayule growth and water use were low (Elshikha et al., 2021). On most RS dates, the RGB drone was flown first at about hour 1200, immediately followed by the MS drone flight. Drones were flown at 61 m above ground level, which provided high spatial resolution.

## 2.3. Guayule plant cover and yield measurements

As described in Elshikha et al. (2021), manual measurements of canopy width (W) were made  $\approx$ once a month in all irrigation treatments. The  $f_c$  (as a percent) was calculated using Eq. (3):

$$f_c (\%) = (W_{ew} \times W_{ns}) / (1/P_d) \times 100 \quad (3)$$

where:

$W_{ew}$  is plant width in the east-west direction, m.

$W_{ns}$  is plant width in the north-south direction, m.

$1/P_d$  is planting area (1/plant density [ $P_d$ ]),  $m^2$ .

<sup>1</sup> Mention of trade names or commercial products in this article is solely for the purpose of providing specific information and does not imply recommendation or endorsement by the U.S. Department of Agriculture. USDA is an equal opportunity provider and employer.

Whole plant samples were harvested in early-Mar. 2020,  $\approx$  23 months after planting. For the plant samples, three 1–3  $m^2$  sections from each plot were hand-harvested at all sites. All plant harvests were limited to the inner four rows of each plot to minimize any border effects on plant growth. Plant samples were prepared and analyzed for resin and rubber concentrations, determined using accelerated solvent extraction and a Soxhlet-based nir spectroscopy method that has high correlation to other rubber analysis methods (Suchat et al., 2013; Placido et al., 2020). The treatment means for final DB, RY, and ReY were provided in Elshikha et al. (2021).

## 2.4. Statistical analysis

The following linear prediction models were developed using measured field experiment data, as well as data of RGB images, TGI, and NDVI, collected from drones:

- 1) NDVI vs TGI, including RS data from late Jun. 2018 (about two months after planting) through early Mar. 2020 (just prior to harvest).
- 2) Measured  $f_c$  (%) vs NDVI and vs TGI, including data from late Jun. 2018 ( $\approx$ 20–25% measured  $f_c$  for all treatments) through early Nov. 2018 when measured maximum  $f_c$  (97–100%) was obtained for all treatments except the D50 (82% average  $f_c$ ).
- 3) Measured  $f_c$  (%) vs estimated  $f_c$  based on RGB images, including data as in 2) above.
- 4) Measured  $K_{cb}$  and  $K_c$  vs NDVI and vs TGI, including data from late Jun. 2018 through early Mar. 2020.
- 5) Measured DB, RY, and ReY vs NDVI and vs TGI, based on the average NDVI and TGI data for each treatment plot (18 plots total) collected during the second year's active growth period (i.e., late Apr. to late Nov. 2019).

All linear regression analyses were computed using the Data Analysis Tools in Microsoft Excel (2019). In addition to the regression coefficient of determination ( $r^2$ ) for evaluating goodness of fit, the root mean square error (RMSE) was calculated as an indicator of the prediction error.

## 3. Results and discussion

### 3.1. NDVI and TGI indices

The NDVI for direct-seeded guayule planted on the sandy loam soil in Maricopa increased rapidly during the first year of growth starting in late Jun. 2018 (Fig. 1a). The NDVI had relatively lower values for the lowest water application rate (D50) and higher values for the highest water application rates (D125–D150). The NDVI reached maximum values (0.77–0.80 for D125 and D150) towards the end of Sep. 2018 and it remained at about the same level until early-Nov. The NDVI then decreased after Nov. 2018 during the winter dormancy period and decreased to a minimum value of about 0.40 in early Feb. 2019. In general, there was no significant difference in the NDVI between the irrigation treatments during the first year of growth. In the second year, however, the irrigation treatments diverged from mid-Apr. to mid-Oct. 2019, which is the period of most active growth (Fig. 1b). The higher irrigation rates (D100–D150 and F100) had the higher NDVI values compared to the lower water treatments (D50–D75). During the second winter dormancy period ( $\approx$  early Nov. 2019 to Mar. 2020), NDVI decreased to values less than 0.40 for treatments and treatment differences were not significant. Sudden decreases in NDVI were observed twice in the second dormancy period (late Oct. to mid-Nov. 2019 and early to mid-Jan. 2020). The rapid reductions in NDVI might have occurred because of a pronounced change in minimum air temperatures during these two periods,  $\approx$  4–6 °C cooler compared to the temperatures in the weeks before and after. Lopez-Bernal et al. (2020) stated that cold-induced dormancy in winter can be reversed after 1–2 weeks of

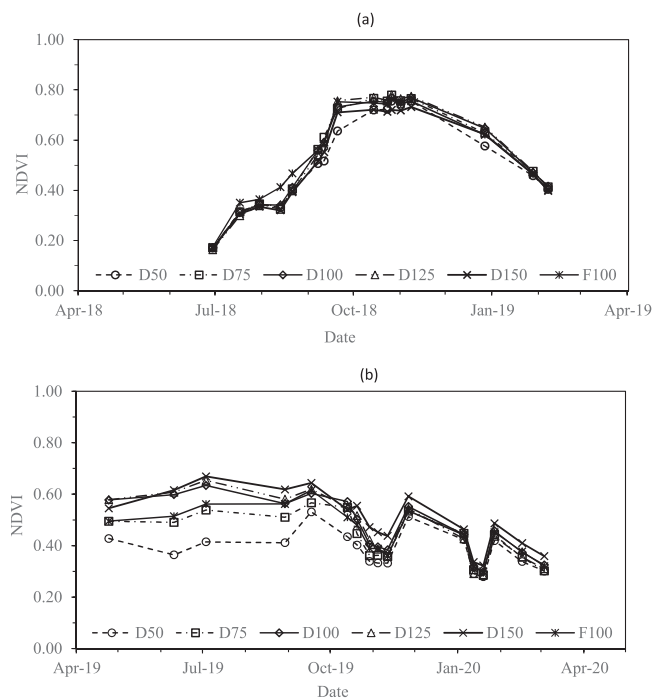


**Fig. 1.** Normalized difference vegetation index (NDVI) for direct-seeded guayule during the first (a) and second (b) years of growth (Jun. 2018-Feb. 2019 and Apr. 2019-Mar. 2020, respectively) in Maricopa, AZ. The letters D and F represent subsurface drip and furrow irrigation, respectively. The numbers following the letters D and F are irrigation rates (i.e., percent replacement of crop evapotranspiration [ET<sub>c</sub>]).

exposure to warm conditions. Therefore, subsequent periods of warmer air temperatures may have caused the plants to temporarily break dormancy and shift into more active growth.

The RS data collected over guayule from late Jun. 2018 to harvest (Mar. 2020) indicated that the NDVI was linearly related to the RGB-based TGI having a regression  $r^2$  of 0.52 and a RMSE of 0.11 (Fig. 2 and Table 1). The slope and intercept coefficients of the model suggest that NDVI will be above the TGI value by about 0.08 early in the season to about 0.14 at maximum TGI values. While the overall trends of NDVI and TGI growth were similar, point to point variations were large. In particular, TGI responded differently when values for NDVI were above 0.70, which occurred during Sep. to Nov. of 2018 (Fig. 1a). The data suggest that the TGI color may have been affected differently by canopy shadows causing errors in separating soil from plant pixels. While Fuentes-Peailillo et al. (2018) also report a general consistency between

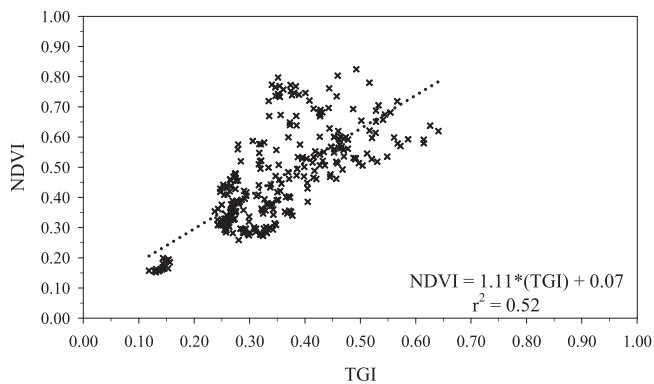


**Fig. 2.** Relationship between NDVI and the RGB-based triangular greenness index (TGI) for direct-seeded guayule during growth periods of the first and second years (i.e., Jun. 2018 through Mar. 2020) in Maricopa, AZ.

**Table 1**

Summarized guayule linear regression equations: normalized difference vegetation index (NDVI) as a function of triangular greenness index (TGI); fractional canopy cover ( $f_c$ ) as functions of NDVI and TGI;  $f_c$  as a function of RGB; basal ( $K_{cb}$ ) and single ( $K_c$ ) crop coefficients as functions of NDVI and TGI; and dry biomass (DB), rubber yield (RY), and resin yield (ReY) as functions of NDVI and TGI. The coefficient of determination ( $r^2$ ) and the root mean square error (RMSE) are shown for each equation.

Parameter	Equation	$r^2$	RMSE	Valid during
NDVI	$NDVI = 0.07 + 1.11 * (TGI)$	0.52	0.11	1st 2 years of growth
$f_c$ (%)	$f_c = 127.8 * (NDVI) - 18.4$	0.90	9.3	early growth to full cover
	$f_c = 212.4 * (TGI) - 19.9$	0.50	19.9	
	$f_c = 1.03 * (f_{c(RGB)}) + 14.5$	0.96	6.8	
$K_{cb}$	$K_{cb} = 1.11 * (NDVI) + 0.39$	0.46	0.19	early growth to harvest
	$K_{cb} = 1.72 * (TGI) + 0.32$	0.48	0.19	
$K_c$	$K_c = 1.11 * (NDVI) + 0.44$	0.41	0.21	
DB (Mg ha <sup>-1</sup> )	$DB = 1.68 * (TGI) + 0.38$	0.40	0.22	harvest <sup>a</sup>
	$DB = 103.5 * (NDVI) - 27.8$	0.75	3.10	
RY (Mg ha <sup>-1</sup> )	$RY = 88.2 * (TGI) - 13.5$	0.72	3.20	
	$RY = 2.61 * (NDVI) - 0.37$	0.53	0.13	
	$RY = 2.17 * (TGI) + 0.02$	0.48	0.32	
ReY (Mg ha <sup>-1</sup> )	$ReY = 8.63 * (NDVI) - 2.13$	0.70	0.29	
	$ReY = 7.25 * (TGI) - 0.89$	0.65	0.31	

<sup>a</sup> Assuming a prototypical late-winter or early spring guayule harvest.

TGI and NDVI data, they point out that RGB data is subject to mis-identifying crop vegetation, particularly in the row zone. Costa et al. (2020), however, reported a visible NDVI based on RGB data that was highly correlated to MS NDVI ( $r^2 = 0.85$  and  $0.82$ ) for all growth periods of citrus and sugarcane crops, respectively. By contrast, the RGB-based indices used by (Marin et al., 2020) did not correlate well with NDVI during the active growing period of turfgrass ( $r^2 = 0.31-0.58$ ). Here, it is indicated that TGI as collected via an inexpensive drone provides a reasonable association with the guayule NDVI data trend, though TGI tends to underestimate the seasonable data spread observed for NDVI.

### 3.2. Remote sensing and guayule cover relationships

The regression model for  $f_c$  vs NDVI was linear with an  $r^2$  value of 0.90 (Fig. 3a) and a RMSE of 9.3% (Table 1). The equation presented is only valid during guayule growth periods prior to canopy closure. Thus, a guayule grower using this NDVI equation to model percent cover would need to visually-assess when the crop is at full cover. Once full cover is achieved, the grower could then assume 100% cover in modeling subsequent irrigation scheduling.

Tenreiro et al. (2021) developed NDVI- $f_c$  regression models with agricultural crop data from 19 different studies, including data of Er-Raki et al. (2007) and Johnson and Trout (2012). They concluded that the models they developed (both linear and quadratic) were adequate for most of the crops presented, as  $r^2$  values were generally above 0.75 and RMSE were less than 20%. In comparison with the Tenreiro et al. (2021) models, the guayule NDVI- $f_c$  model appears to be as statistically robust to those developed for many agricultural crops. In particular, the linear equation in Fig. 3a has similar regression coefficients to those reported by Johnson and Trout (2012), obtained for a variety of vegetable crops, as well as to those reported for cotton (Neale et al., 2021).

The equation of  $f_c$  vs TGI had an  $r^2 = 0.50$  and RMSE = 20.9%

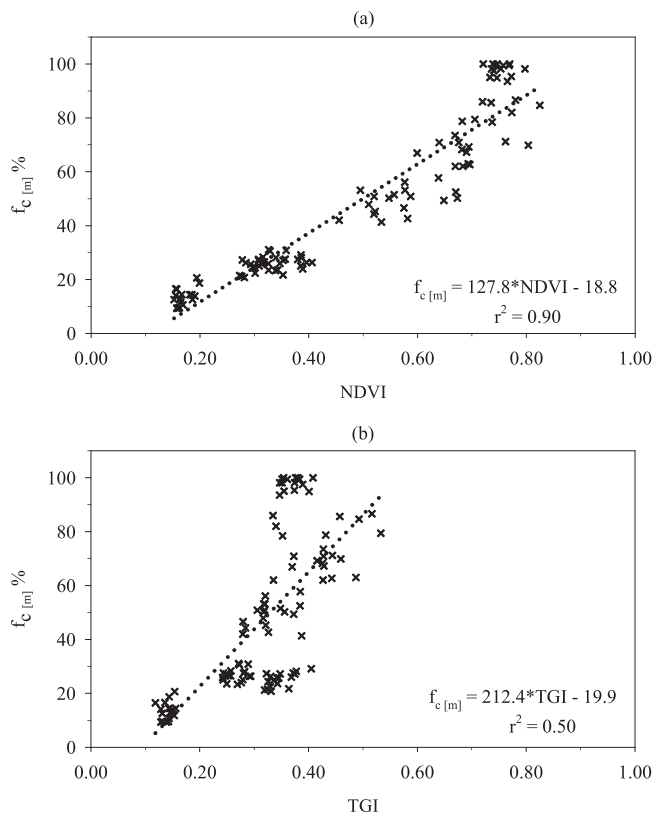


**Fig. 3.** Fractional canopy cover (manually measured,  $f_c [m]$ ) vs. NDVI (a) and TGI (b) for direct-seeded guayule through canopy closure during the first year (late Jun.-early Nov. 2018) in Maricopa.

(Fig. 3b and Table 1). Thus, the RMSE for  $f_c$  vs TGI was over twice that for  $f_c$  vs NDVI. Since TGI did not correlate strongly with NDVI, it was expected that the  $f_c$  vs TGI relationship would be less effective than  $f_c$  vs NDVI. Problems resulted due to the mismatch of TGI with  $f_c$  during early-season (25–30% measured  $f_c$ ) and a decline in TGI when measured  $f_c$  reached 92–100% in plots. As indicated earlier, the TGI has been found to be prone to errors in soil and vegetation identification (Fuentes-Peailillo et al., 2018).

Manually measured  $f_c$  vs. RGB-based cover ( $f_{c\text{ RGB}}$ ) during the first year of growth is illustrated in Fig. 4. The linear equation had an  $r^2$  value

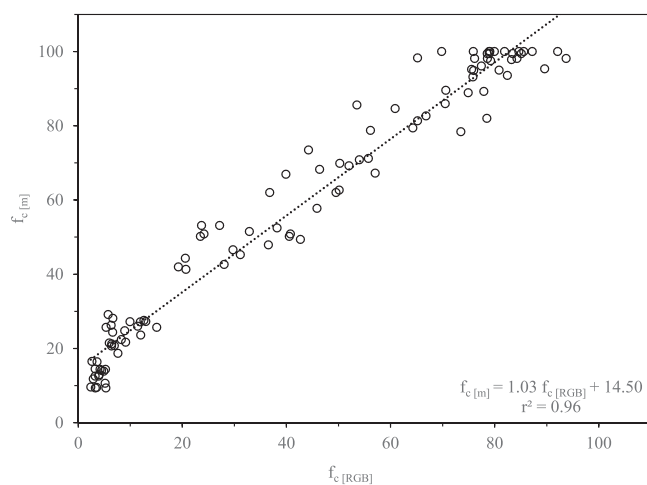


**Fig. 4.** Fractional canopy cover (manually measured,  $f_c [m]$ ) vs. RGB-based  $f_c$  ( $f_c [RGB]$ ) for direct seeded guayule during the first year's active growth period (Apr.-Nov. 2019) in Maricopa.

of 0.96 with a RMSE of 6.8% (Table 1). Since  $f_{c\text{ RGB}}$  is based on the hue values, or plant greenness, it followed guayule canopy cover development well during the first year. While the linear fit was good, the  $f_{c\text{ RGB}}$  model under-estimated the measured  $f_c$  and thus it does not quantify the measured  $f_c$  adequately. Others, such as Lee and Lee (2011) with rice and Ashapure et al. (2019) with cotton, developed similar RGB-based  $f_c$  models. Contrary to the guayule model, those studies reported near 1:1 relationships between measured and the RGB-based models. The cotton study (Ashapure et al., 2019) indicated RMSE of estimated  $f_c$  less than 3%. Both studies recommended that RGB-based estimation of  $f_c$  can be used as an affordable alternative to MS-based models.

### 3.3. NDVI- and TGI-based crop coefficients

Linear curves of  $K_{cb}$  vs NDVI and  $K_c$  vs NDVI, developed using data from late Jun. 2018 through early Mar. 2020, are shown in Fig. 5a and b, respectively. The  $r^2$  were 0.46 and 0.41 and RMSE were 0.19 and 0.21 for  $K_{cb}$  and  $K_c$ , respectively (Table 1). The initial NDVI measurements in late Jun. 2018 were slightly less than 0.20 and corresponded to crop coefficient values of about 0.62 and 0.67 for  $K_{cb}$  and  $K_c$ , respectively. Maximum values for  $K_{cb}$  during the first year growing period occurred between mid-Sep. to early Nov. 2018 and averaged 1.16, corresponding to maximum NDVI values of about 0.75 (Fig. 5a). Appreciable soil evaporation occurred for the F100 (furrow) treatment on several dates during the first year growing period leading to some high values for  $K_c$  (1.19–1.35) prior to mid-Sep. 2018 (Fig. 5b). During the guayule winter dormancy periods in 2018–2019 and 2019–2020 (late Nov. to early Mar.), NDVI were at minimum values (typically 0.30–0.50), whereas  $K_{cb}$  values varied from about 0.45–1.25 during these periods. Thus, much of

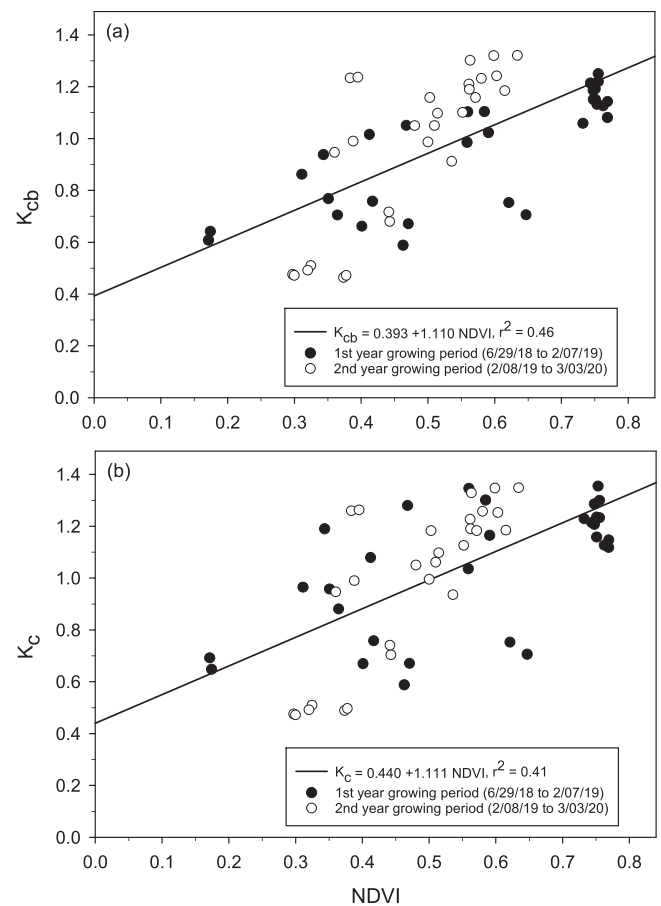


**Fig. 5.** Basal and single crop coefficient ( $K_{cb}$  and  $K_c$ ) as a function of NDVI for direct-seeded guayule during the two years of growth (June 2018-Mar. 2020) in Maricopa.

the scatter about the curves is due to a discontinuity of the relationship between  $K_{cb}$  and NDVI during winter dormancy (i.e., generally, the values falling below the curve fits) versus the active growing periods (i.e., values near or above the curve fits). Generally, the NDVI tracked  $K_{cb}$  somewhat better than  $K_c$  because of the incidence of early season soil evaporation for the F100 treatment. Despite the positive intercepts for the  $K_{cb}$  and  $K_c$  vs NDVI equations, the regression slopes (1.10–1.11) are consistent with NDVI relationships for other crops, e.g.,  $K_{cb}$  of 1.09 for corn (Neale et al., 1989) and 1.07 for wheat (Er-Raki et al., 2007).

The  $K_{cb}$  and  $K_c$  vs TGI relationships (Figs. 6a and 6b, respectively, and Table 1) were comparable to those for NDVI in terms of the  $r^2$  (0.48 and 0.40, respectively) and RMSE (0.19 and 0.22, respectively). This result was somewhat surprising given the differences between NDVI and TGI (Fig. 2) and the better relationship of  $f_c$  vs NDVI than vs TGI through early Nov. 2018 when full cover for treatments occurred (Figs. 3a and 3b, respectively). However, highest  $K_{cb}$  occurred during the spring-summer of the second year growing period (2019–2020). In that period, NDVI values declined appreciably compared to those observed in Sep.-Nov. 2018. On the other hand, TGI declined to a lesser extent during spring-summer compared to TGI values observed in Sep.-Nov. 2018. In general, TGI appeared to be in better agreement with the higher  $K_{cb}$  values during both the first- and second-year growing periods compared to NDVI. Comparative studies that assess the crop coefficient as a function of both NDVI and TGI were not found in the literature.

### 3.4. Prediction of guayule yields

The regression equations for final dry biomass (DB), rubber yield

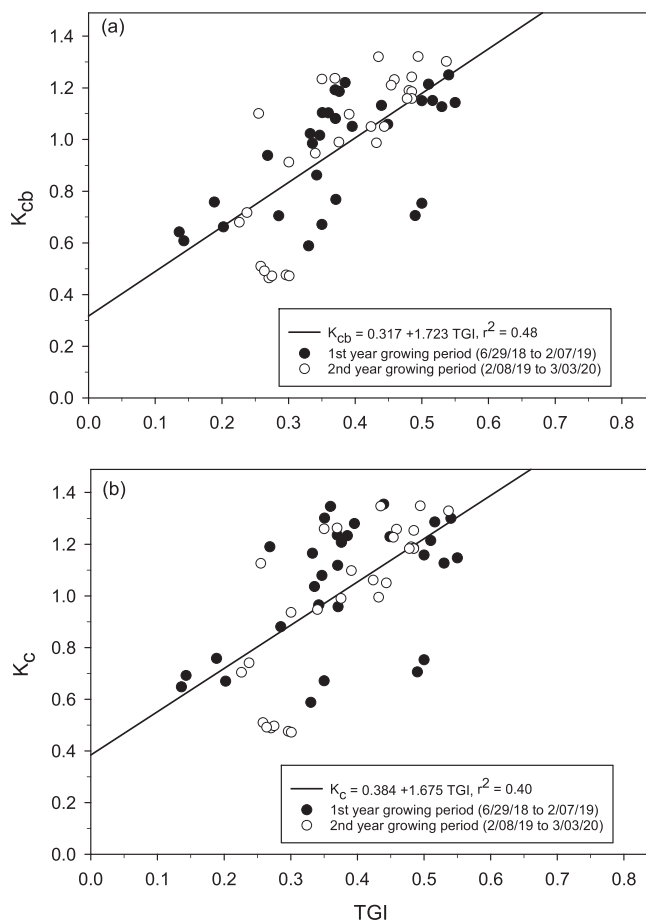


Fig. 6. Basal and single crop coefficient ( $K_{cb}$  and  $K_c$ ) as a function of TGI for direct-seeded guayule during the two years of growth (June 2018–Mar. 2020) in Maricopa.

(RY), and resin yield (ReY) as functions of NDVI and TGI are given in (Figs. 7 and 8, respectively, and Table1). Both the MS and RGB indices were robust indicators of DB, as evidenced by  $r^2$  values for NDVI and TGI of 0.75 and 0.72, respectively, and RMSE less than  $3.2 \text{ Mg ha}^{-1}$  (or about a 10% error). As expected, the NDVI and TGI fits were not as precise for ReY ( $r^2 = 0.70$  and  $0.65$ , respectively) and RY ( $r^2 = 0.53$  and  $0.48$ , respectively) compared to the DB equations. The imprecision occurs because the indices cannot detect the differences in resin or rubber content. Still, the NDVI and TGI equations gave reasonable estimates of measured rubber and resin yields (within about 10–30% of measured). However, an ability of NDVI and TGI indices to adequately estimate the guayule DB ahead of final harvest would be useful information for guayule growers in terms of planning harvest and post-harvest operations.

### 4. Conclusions

The study examined the use of multispectral (MS) and RGB indices to estimate plant cover, crop coefficients, and final yields of direct-seeded guayule in the U.S. Southwest. The results indicate that RGB (TGI) and MS NDVI data collected by drone could provide valuable assistance for managing guayule irrigation and a priori estimation of final yields. The NDVI was highly correlated to plant cover fraction during the first year of growth, prior to treatments achieving full cover. Additionally, it was shown that NDVI and TGI gave reasonable estimated guayule crop coefficients during the two years of growth, including the winter dormancy period when the crop coefficients rapidly decline, as well as during the following active growing period. We conclude that the NDVI-based plant cover and TGI-based crop coefficient models could be used with reasonable confidence in guayule production fields in different areas of the U.S. Southwest. These crop parameters are essential inputs in determining crop evapotranspiration and irrigation requirements. Thus, the predictive capabilities of these parameters by NDVI and TGI data from drone would be a significant asset for managing guayule irrigation and optimization of agronomic production. As an alternative to using MS sensors for NDVI, less expensive RGB camera data could be used to estimate guayule NDVI by the provided NDVI vs TGI equation. However, this equation should be used with caution since NDVI was generally underestimated to some extent by TGI during the two years of guayule growth. The NDVI (or TGI) prediction equations of dry biomass, rubber yield, and resin yield provide information needed in planning harvest and post-harvest operations, such as labor, transportation, and storage, as well as planning rubber and resin extraction, which are time sensitive. The rate of advances in drones and sensor manufacturing technologies are expected to increase, while cost is expected to be reduced. These factors will help increase the viability and use of drone-sensor packages for guayule agronomic management and yield prediction.

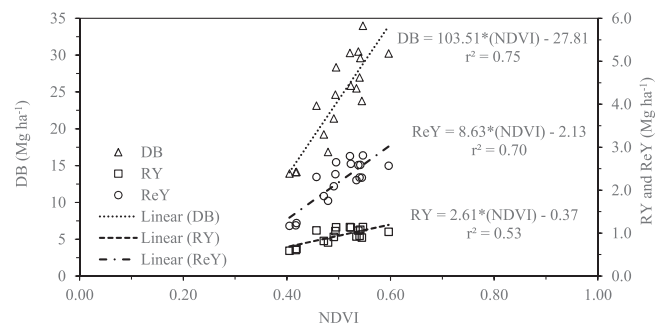
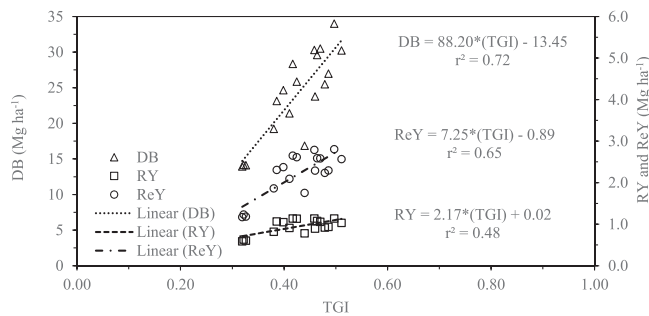


Fig. 7. Prediction of dry biomass (DB), rubber yield (RY) and resin yield (ReY) using mid-season (April–Nov 2019) NDVI data for direct-seeded guayule grown in Maricopa.



**Fig. 8.** Prediction of dry biomass (DB), rubber yield (RY) and resin yield (ReY) using mid-season (April–Nov 2019) triangular vegetation index [RGB based] (TGI) data for direct-seeded guayule grown in Maricopa.

### Declaration of Competing Interest

The authors declare that they have no known competing financial interests or personal relationships that could have appeared to influence the work reported in this paper.

### Acknowledgments

The authors thank Bridgestone Americas, Inc. for providing the guayule seeds and assistance in planting and harvesting. We thank Stefan Dittmar and Russell Prock, with Bridgestone Americas, and Allan Knopf and Matt Hagler, with USDA, for field and drone technical support, Ahmed El-Sheikha for help with field irrigation and data collection, and Theresa Sullivan, Bridgestone Americas for shrub processing and rubber, resin, and moisture analysis. This project was supported by Sustainable Bioeconomy for Arid Regions (SBAR), USDA National Institute of Food and Agriculture (NIFA), USA Grant no. 2017-68005-26867.

### References

- Allen, S.G., Nakayama, F.S., Dierig, D.A., Rasnack, B.A., 1987. Plant water relations, photosynthesis, and rubber content of young guayule plants during water stress. *Agron. J.* 79, 1030–1035.
- Allen, R.G., Pereira, L.S., Raes, D., Smith, M., 1998. *Crop Evapotranspiration*. Food and Agric. Org. of the United Nations, Rome, Italy. FAO Irrigation and Drainage Paper 56.
- Ashpore, A., Jung, J., Chang, A., Oh, S., Maeda, M., Landivar, J., 2019. A comparative study of RGB and multispectral sensor-based cotton canopy cover modelling using multi-temporal UAS data. *Remote Sens.* 11, 2757.
- Bausch, W.C., Neale, C.M.U., 1989. Spectral inputs improve corn crop coefficients and irrigation scheduling. *Trans. ASAE* 32 (6), 1901–1908.
- Bausch, W.C., 1995. Remote sensing of crop coefficients for improving the irrigation scheduling of corn. *Agric. Water Manag.* 27 (1), 55–68.
- Brandao, Z.N., Sofiatti, V., Bezerra, J.R.C., Ferreira, G.B., Medeiros, J.C., 2015. Spectral reflectance for growth and yield assessment of irrigated cotton. *Aust. J. Crop Sci.* 9 (1), 75–84.
- Chen, J., Yi, S., Qin, Y., Wang, X., 2016. Improving estimates of fractional vegetation cover based on UAV in alpine grassland on the Qinghai-Tibetan Plateau. *Int. J. Remote Sens.* 37, 1922–1936.
- Campos, J., Llop, J., Gallart, M., Garcia-Ruiz, F., Gras, A., Salcedo, R., Gil, E., 2019. Development of canopy vigour maps using UAV for site-specific management during vineyard spraying process. *Precis. Agric.* 1136–1156.
- Coelho, A.P., Rosalen, D.L., de Faria, R.R., 2018. Vegetation indices in the prediction of biomass and grain yield of white oat under irrigation levels. *Pesq. Agropec. Trop.* 48 (2), 109–117.
- Coffelt, T.A., Ray, D.T., 2010. Cutting height effects on guayule latex, rubber, and resin yields. *Ind. Crops Prod.* 32, 264–268.
- Cornish, K., Pearson, C.H., Rath, D.J., 2013. Accurate quantification of guayule resin and rubber requires sample drying below a critical temperature threshold. *Ind. Crops Prod.* 41, 158–164.
- Costa, L., Nunes, L., Ampatzidis, Y., 2020. A new visible band index (vNDVI) for estimating NDVI values on RGB images utilizing genetic algorithms. *Comput. Electron. Agric.* 172, 105334.
- Downes, R.W., Tonnet, M.L., 1985. Effect of environmental conditions on growth and rubber production of guayule (*Parthenium argentatum*). *Aust. J. Agric. Res.* 36, 285–294.

- Duan, T., Zheng, B., Guo, W., Ninomiya, S., Guo, Y., Chapman, S.C., 2017. Comparison of ground cover estimates from experiment plots in cotton, sorghum and sugarcane based on images and ortho-mosaics captured by UAV. *Funct. Plant Biol.* 44, 169.
- Elshikha, D.E.M., Waller, P.M., Hunsaker, D.J., Dierig, D.A., Wang, G., Cruz, V.M.V., Thorp, K.R., Katterman, M.E., Bronson, K.F., Wall, G.W., 2021. Growing direct-seeded guayule with furrow and subsurface drip irrigation in Arizona. *Ind. Crops Prod.* 170, 113819.
- Er-Raki, S., Chehbouni, A., Guemouria, N., Duchemin, B., Ezzahar, J., Hadria, R., 2007. Combining FAO-56 model and ground-based remote sensing to estimate water consumptions of wheat crops in a semi-arid region. *Agric. Water Manag.* 87, 41–54.
- Fuentes-Peailillo, F., Ortega-Farías, S., Rivera, M., Bardeen M., Moreno, M., 2018. Comparison of vegetation indices acquired from RGB and Multispectral sensors placed on UAV. *IEEE International Conference on Automation/XXIII Congress of the Chilean Association of Automatic Control (ICA-ACCA)*, 1–6, doi: 10.1109/ICA-ACCA.2018.8609861.
- Hlatshwayo, S.T., Mutanga, O., Lottering, R.T., Kiala, Z., Ismail, R., 2019. Mapping forest aboveground biomass in the reforested Buffelsdraai landfill site using texture combinations computed from SPOT-6 pan-sharpened imagery. *Int. J. Appl. Earth Obs.* 74, 65–77.
- Huang, Y., Brand, H.J., Sui, R., Thomson, S.J., Furukawa, T., Ebelhar, M.W., 2016. Cotton yield estimation using very high-resolution digital images acquired with a low-cost small unmanned aerial vehicle. *Trans. ASABE* 59 (6), 1563–1574.
- Hunsaker, D.J., Barnes, E.M., Clarke, T.R., Fitzgerald, G.J., Pinter Jr, P.J., 2005. Cotton irrigation scheduling using remotely sensed and FAO-56 basal crop coefficients. *Trans. ASAE* 48 (4), 1395–1407.
- Hunsaker, D.J., Elshikha, D.M., 2017. Surface irrigation management for guayule rubber production in the US desert Southwest. *Agric. Water Manag.* 185, 43–57.
- Hunt Jr, E.R., Cavigelli, M., Daughtry, C.S.T., McMurtrey, J.E., Walthall, C.L., 2005. Evaluation of digital photography from model aircraft for remote sensing of crop biomass and nitrogen status. *Precis. Agric.* 6, 359–378.
- Hunt Jr, E.R., Daughtry, C.S.T., Eitel, J.U.H., Long, D.S., 2011. Remote sensing leaf chlorophyll content using a visible band index. *Agron. J.* 103, 1090–1099.
- Hunt Jr, E.R., Doraiswamy, P.C., McMurtrey, J.E., Daughtry, C.S.T., Perry, E.M., Akhmedov, B., 2013. A visible band index for remote sensing leaf chlorophyll content at the canopy scale. *Int. J. Appl. Earth Obs. Geoinf.* 21, 103–112.
- Ji, Z., Pan, Y., Zhu, X., Wang, J., Li, Q., 2021. Prediction of crop yield using phenological information extracted from remote sensing vegetation index. *Sensors* 21 (4), 1406.
- Jiang, X., Gao, M., Gao, Z., 2020. A novel index to detect green-tide using UAV-based RGB imagery. *Estuar. Coast. Shelf Sci.* 245, 106943.
- Jayanthi, H., Neale, C.M.U., Wright, J.L., 2001. Seasonal evapotranspiration estimation using canopy reflectance: A case study involving pink beans. In: Owe, M., Brubaker, K., Ritchie, J., Rango, A. (Eds.), *Proc. Int. Symp. Remote Sensing and Hydrology 2000*, 302–305. IAHS Press, Wallington, Oxfordshire, U.K.
- Johnson, L.F., Roczen, D.E., Youkhana, S.K., Nemani, R.R., Bosch, D.F., 2003. Mapping vineyard leaf area with multispectral satellite imagery. *Comput. Electron. Agric.* 38, 33–44.
- Johnson, L.F., Trout, T.J., 2012. Satellite NDVI assisted monitoring of vegetable crop evapotranspiration in California's San Joaquin Valley. *Remote Sens.* 4, 439–455.
- Kanning, M., Kuhlring, I., Trautz, D., Jarmer, T., 2018. High-Resolution UAV-Based hyperspectral imagery for LAI and chlorophyll estimations from wheat for yield prediction. *Remote Sens.* 10 (12), 2000.
- Lahmers, T., Eden, S., 2018. *Water and irrigated agriculture in Arizona*. Arroyo, Water resources research center, college of agriculture & life sciences, cooperative extension (wrrc.arizona.edu).
- Lee, K.J., Lee, B.W., 2011. Estimating canopy cover from color digital camera image of rice field. *J. Crop. Sci. Biotechnol.* 14, 151–155.
- Li, G., Wan, S., Zhou, J., Yang, Z., Qin, P., 2010. Leaf chlorophyll fluorescence, hyper spectral reflectance, pigments content, malondialdehyde and proline accumulation responses of castor bean (*Ricinus communis* L.) seedlings to salt stress levels. *Ind. Crops Prod.* 31, 13–19.
- Li, S., Ding, X., Kuang, Q., Ata-Ui-Karim, S.T., Cheng, T., Liu, X., Tian, Y., Zhu, Y., Cao, W., Cao, Q., 2018a. Potential of UAV-based active sensing for monitoring rice leaf nitrogen status. *Front. Plant Sci.* 9, 1834.
- Li, L., Mu, X., Macfarlane, C., Song, W., Chen, J., Yan, K., Yan, G., 2018b. A half-Gaussian fitting method for estimating fractional vegetation cover of corn crops using unmanned aerial vehicle images. *Agric. For. Meteorol.* 262, 379–390.
- Lopez-Bernal, A., Garcia-Tejerab, O., Testic, L., Orgaz, F., Villalobos, F.J., 2020. Studying and modelling winter dormancy in olive trees. *Agric. For. Meteorol.* 280, 107776.
- Lu, D., 2005. Aboveground biomass estimation using Landsat TM data in the Brazilian Amazon. *Int. J. Remote Sens.* 26 (12), 2509–2525.
- Marin, J., Yousfi, S., Mauri, P.V., Parra, L., Lloret, J., Masaguer, A., 2020. RGB vegetation indices, NDVI, and biomass as indicators to evaluate C<sub>3</sub> and C<sub>4</sub> turfgrass under different water conditions. *Sustainability* 12, 2160.
- Mondal, P., Basu, M., 2009. Adoption of PA technologies in India and some developing countries: scope, present status and strategies. *Prog. Nat. Sci.* 19, 659–666.
- Mpanga, I.K., Idowu, O.J., 2021. A Decade of Irrigation Water use trends in Southwestern USA: the role of irrigation technology, best management practices, and outreach education programs. *Agric. Water Manag.* 243, 106438.
- Neale, C.M.U., Bausch, W.C., Heermann, D.E., 1989. Development of reflectance-based crop coefficients for corn. *Trans. ASAE* 32 (6), 1891–1899.
- Neale, C.M.U., Jayanthi, H., and Wright, J.L., 2003. Crop and irrigation water management using high-resolution airborne remote sensing. In *Proc. ICID Workshop Remote Sensing of ET for Large Regions, CD-ROM*. New Delhi, India: International Commission on Irrigation and Drainage.

- Neale, C.M.U., Gonzalez-Dugo, M.P., Serrano-Perez, A., Campos, I., Mateos, L., 2021. Cotton canopy reflectance under variable solar zenith angles: Implications of use in evapotranspiration models. *Hydrol. Process.* 35, 14162.
- Placido, D.F., Dierig, D.A., Cruz, V.M.V., Ponciano, G., Dong, C., Dong, N., Huynh, T., Williams, T., Cahoon, R.E., Wall, G.W., Wood, D.F., McMahan, C., 2020. Downregulation of an allene oxide synthase gene improves photosynthetic rate and alters phytohormone homeostasis in field-grown guayule. *Ind. Crops Prod.* 153, 112341 <https://doi.org/10.1016/j.indcrop.2020.112341>.
- Pocas, I., Calera, A., Campos, I., Cunha, M., 2020. Remote sensing for estimating and mapping single and basal crop coefficients: a review on spectral vegetation indices approaches. *Agric. Water Manag.* 223, 106081.
- Ray, D.T., Foster, M.A., Coffelt, T.A., McMahan, C., 2010. Guayule: Culture, breeding and rubber production. *Industrial Crops and Uses*. CAB International, Massachusetts, pp. 384–410.
- Suchat, S., Pioch, D., Palu, S., Tardan, E., van Loo, E.N., Davrieux, F., 2013. Fast determination of the resin and rubber content in *Parthenium argentatum* biomass using near infrared spectroscopy. *Ind. Crops Prod.* 45, 44–51.
- Tenreiro, T.R., Garcia-Vila, M., Gomez, J.A., Jimenez-Berni, J.A., 2021. Using NDVI for the assessment of canopy cover in agricultural crops within modelling research. *Comput. Electron. Agric.* 182, 106038.
- Thorp, K.R., Dierig, D.A., 2011. Color image segmentation approach to monitor flowering in *lesquerella*. *Ind. Crops Prod.* 34, 1150–1159.
- Torres-Sanchez, J., Pena, J.M., de Castro, A.I., Lopez-Granados, F., 2014. Multi-temporal mapping of the vegetation fraction in early-season wheat fields using images from UAV. *Comput. Electron. Agric.* 103, 104–113.
- Tucker, C.J., 1979. Red and photographic infrared linear combinations for monitoring vegetation. *Remote Sens. Environ.* 8, 127–150.
- Vina, A., Gitelson, A.A., Rundquist, D.C., Keydan, G., Leavitt, B., Schepers, J., 2004. Monitoring maize (*Zea mays* L.) phenology with remote sensing. *Agron. J.* 96 (4), 1139–1147.
- Xu, W., Yang, W., Chen, S., Wu, C., Chen, P., Lan, Y., 2020. Establishing a model to predict the single boll weight of cotton in northern Xinjiang by using high resolution UAV remote sensing data. *Comput. Electron. Agric.* 179, 105762.
- Yan, G., Li, L., Coy, A., Mu, X., Chen, S., Xie, D., Zhang, W., Shen, Q., Zhou, H., 2019. Improving the estimation of fractional vegetation cover from UAV RGB imagery by colour unmixing. *ISPRS J. Photogramm. Remote Sens.* 158, 23–34.
- Yang, M., Hassan, M.A., Xu, K., Zheng, C., Rasheed, A., Zhang, Y., Jin, X., Xia, X., Xiao, Y., He, Z., 2020. Assessment of water and nitrogen use efficiencies through UAV-Based multispectral phenotyping in winter wheat. *Front. Plant Sci.* 11, 927.
- Zhao, D., Reddy, K.R., Kakani, V.G., Read, J.J., Koti, S., 2007. Canopy reflectance in cotton for growth assessment yield prediction. *Eur. J. Agron.* 26, 335–344.
- Zhang, J., Qiu, X., Wu, Y., Zhu, Y., Cao, Q., Liu, X., Cao, W., 2021. Combining texture, color, and vegetation indices from fixed-wing UAS imagery to estimate wheat growth parameters using multivariate regression methods. *Comput. Electron. Agric.* 185, 106138. June 2021.